Unusually Long-Time Protonic Conductivity Behavior of $CsH_5(PO_4)_2$ Crystal at High Pressure

M. Zdanowska-Frączek[a,*] and T. Masłowski[b]

[a] *Institute of Molecular Physics, Polish Academy of Sciences, Smoluchowskiego 17, 60-179 Poznań, Poland*
[b] *The Faculty of Mathematics and Applied Physics, Rzeszow University of Technology, al. Powstańców Warszawy 6, 35 959 Rzeszów, Poland*

Received: 21.10.2025 & Accepted: 22.12.2025

Doi: 10.12693/APhysPolA.148.295 *e-mail: mzf@impan.poznan.pl

Impedance spectroscopy was used to examine the electrical conductivity of $CsH_5(PO_4)_2$ single crystals across a frequency range from 100 Hz to 1 MHz, with measurements taken at temperatures from 350 to 417 K and pressures from 0.1 to 360 MPa. At 417 K and 170.7 MPa, the protonic conductivity of the crystal showed significant changes over time. Initially, conductivity remained relatively stable for less than 10 h; however, it increased tenfold within 300 h, exhibiting erratic fluctuations followed by a gradual decline. We suggest a three-dimensional model of protonic conductivity that qualitatively reproduces the observed behavior.

topics: $CsH_5(PO_4)_2$, proton conductivity, impedance spectroscopy, high pressure

1. Introduction

Alkaline metal phosphates (MPs), including cesium pentahydrogen phosphate, comprise diverse acidic solids with unique properties. These characteristics render them suitable for various applications, such as catalysts [1–3], fuel cells [4–6], batteries [7], and biomedicine [8]. The crystalline forms of these solids can vary significantly depending on the metal/phosphate combination and the synthesis method employed. A fascinating subgroup of these compounds is the family of solid acids, which exhibit highly conductive phases and dynamically disordered hydrogen bond networks. In solid acids, protons can migrate only within these hydrogen bond networks. Transport occurs with minimal activation energy through a Grotthuss-type mechanism [9]. This process is two-stage, dynamic, and cooperative, involving protons jumping from one potential minimum to another within a hydrogen bond (intrachain H^+ transport, at a rate of about 10^{-9} s) and reorientation of their immediate surroundings (XO_4 reorientations), which leads to interchain H^+ transport lasting from 10^{-11} to 10^{-12} s. Since the Grotthuss mechanism involves two processes, two activation energies must be considered. Molecular dynamics and Monte Carlo simulations have demonstrated that the activation energy for proton displacement within a hydrogen bond is a fraction of the total energy of the process. The key factor for long-range displacement is the ratio of the molecular rotation frequency to the frequency of hydrogen bond formation and breaking [10].

The rate of proton movement depends primarily on the hydrogen-bond potential in which the protons are trapped, and therefore on the lengths and angles of the hydrogen bonds forming the sublattice. The conductivity of these salts is anisotropic. Specifically, the electrical conductivity of crystals with the formula $M_3H(XO_4)_2$, where M represents K, Rb, Cs, or NH_4, and X denotes P, S, or Se, shows this anisotropic behavior [11–20].

Most solid acids undergo a superprotonic phase transition, characterized by an increase in conductivity, which reaches values between 10^{-3} and 10^{-2} S/cm. However, the conductivity in the direction perpendicular to the plane of maximum conductivity, i.e., along the c axis of the crystal, is several orders of magnitude lower. This discrepancy results from the lack of a direct charge transport path in this direction. The large distances separating successive planes of maximum conductivity in the crystal and the presence of monovalent cations do not participate in the formation of hydrogen bonding. In 1996, Merinov et al. [21, 22] proposed the formation of "supplementary" hydrogen bonds involving oxygen atoms from the XO_4 groups of adjacent layers. These "supplementary" bonds are

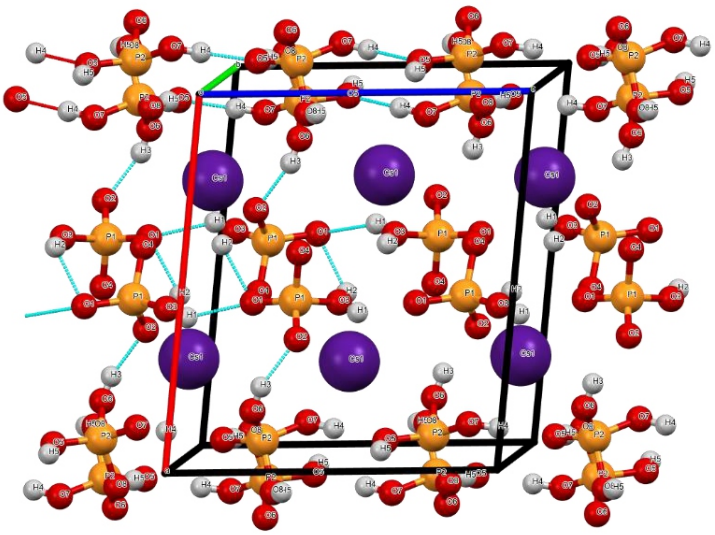

Fig. 1. The structure of the room-temperature phase of $CsH_5(PO_4)_2$, based on structural data from Efremov et al. [23]. Crystallographic Information File (CIF) data available at [24].

located between well-conducting layers. Although the likelihood of these hydrogen bonds forming and occupying in complementary positions is lower than in well-conducting planes, they nonetheless create infinite pathways for proton diffusion along the c direction. This allows protons to migrate from one oxygen atom to another due to the relatively small ($\sim 30°$) libration of XO_4.

This paper investigates the ionic salt $CsH_5(PO_4)_2$, which is closely related to the well-known proton-conductive salt CsH_2PO_4. Efremov et al. [23] analyzed the crystal structure of $CsH_5(PO_4)_2$. At room temperature, the crystal is monoclinic, with a $P21/c$ space group and lattice parameters of $a = 10.879$ Å, $b = 7.768$ Å, $c = 9.536$ Å, $\beta = 96.60°$, and $Z = 4$. This compound features a distinctive hydrogen bond network connecting PO_4^{3-} anions through O-H...O bonds at each corner of the tetrahedra, forming $\{[H_2PO_4]\}_\infty$ in the [001] direction. Electrostatic interactions with Cs^+ ions and one of the hydrogen bonds connect the layers, creating a layered crystal structure. Each formula unit contains five strong hydrogen bonds aligned along the three crystallographic axes. Four of these hydrogen bonds are within the $\{[H_2PO_4]\}_\infty$ plane. Hydrogen bonds are roughly aligned along three crystallographic axes (see Fig. 1) [24]. The four bonds are similar in length, measuring from 0.254 to 0.259 nm in the [010] direction and from 0.253 to 0.254 nm in the [001] direction, while the bond in the [100] direction is shorter at 0.243 nm.

Lavrova et al. [25] conducted initial studies on the transport and thermodynamic properties at atmospheric pressure. The research showed that the conductivity in the crystal exhibits minimal anisotropy, with protons acting as charge carriers. Electric charges are transferred via a Grotthuss-type mechanism. The unique structure of hydrogen bond network contributes to the anisotropic electrical conductivity, with the lowest values observed in the direction perpendicular to the $\{[H_2PO_4]\}_\infty$ layers. The conductivity levels seen in both $CsH_5(PO_4)_2$ single crystals and polycrystalline samples are relatively low and unsuitable for fuel cell applications. Lavrova et al. [25] also suggested that although the transition to a superprotonic disordered phase in the $CsH_5(PO_4)_2$ crystal has not been observed, such a phase might exist at high pressure in acidic salts. As Sinitsin et al. [26] demonstrated, $Rb_3H(SO_4)_2$ is an example of such a material, where the superprotonic phase appears only at high pressure.

The analysis of the ^1H nuclear magnetic resonance (NMR) spectrum and spin-lattice relaxation rates reported in [27] shows that the temperature-dependent hydrogen dynamics in $CsH_5(PO_4)_2$ involve jumps within hydrogen bonds (intra-H-bond) and between hydrogen bonds (inter-H-bond) as the temperature increases. This processes function as an ionic conduction mechanism similar to what is observed in other hydrogen-bonded superprotonic salts. Therefore, studies of $CsH_5(PO_4)_2$ should be performed at high temperatures, because conduction requires not only appropriate hydrogen-bond lengths but also the dynamic motion of the PO_4 groups forming the transport pathways. The dynamics of the groups forming the transport pathways will affect bond lengths and modify the hydrogen-bond potential in which the proton is trapped. The $CsH_5(PO_4)_2$ crystal contains short hydrogen bonds that connect the strongly bound PO_4 groups into $\{[H_2PO_4]\}_\infty$ planes in the [001] direction. Short hydrogen bonds and electrostatic interactions with the cesium cations link these

planes. Both hydrogen bonds and electrostatic interactions are the weakest bonds in crystal structures. The relatively weak bonding between the $\{[H_2PO_4]\}_\infty$ planes causes these bonds to be thermally broken. As a result, the crystal melts before it can reach the open-structure phase characteristic of the superprotonic state.

Andriyevsky et al. [28] performed an *ab initio* density functional theory (DFT) analysis of the $CsH_5(PO_4)_2$ crystal, focusing on its electronic band structure and density of states as the unit cell volume varies with pressure. The research examined properties related to hydrostatic compression and provided insights into electronic states and electric charges, which are essential for understanding the crystal's proton conductivity. The findings suggest that electron–phonon interactions can significantly localize thermal energy, facilitating the release of hydrogen cations, which are vital for proton conductivity in $CsH_5(PO_4)_2$.

The present study aims to examine the proton-conducting crystal $CsH_5(PO_4)_2$ using impedance spectroscopy under various thermodynamic conditions. The goal is to determine whether subtle changes in the crystal structure and proton dynamics caused by a change in thermodynamic conditions can induce a transition to a highly conducting phase in the crystal. We suggest a three-dimensional model of protonic conductivity that qualitatively reflects the observed behavior.

This is the first study presenting impedance spectra recorded under various thermodynamic conditions and over time.

2. Materials and methods

The crystals for the study were provided by Professor V.G. Ponomareva and Dr. G.V. Lavrova from the Institute of Solid State Chemistry, Siberian Branch of the Russian Academy of Sciences in Novosibirsk. Lavrova et al. [25] originally described this method for preparing single crystals. Colorless and transparent crystals of $CsH_5(PO_4)_2$ were grown from an aqueous solution of Cs_2CO_3 and H_3PO_4 in a molar ratio of 1:2 through isothermal evaporation at room temperature. For conductivity measurements, the crystals were cut into plates with faces oriented perpendicular to the [100] direction, which is aligned with the $\{[H_2PO_4]\}_\infty$ layers. The plate-like samples were arranged so that [100] orientation was facing the measurement apparatus.

To prepare the samples for measurement, they were coated with gold electrodes and positioned between two parallel gold plates. The measuring capacitor containing the sample was then placed inside a beryllium bronze pressure chamber filled with helium gas. This pressure chamber was subsequently installed in an Oxford flow cryostat.

The pressures in the chamber were generated using a three-stage helium gas compressor and were measured to an accuracy of 0.2 MPa using a manganin gauge. This gauge was previously calibrated through the pressure-induced phase transition of bismuth, in conjunction with a Keithley 2400 Source Meter. Temperature stabilization was achieved with an Oxford Instruments automatic controller (ITC4), and temperature was measured to an accuracy of ± 0.02 K using a Pt100 sensor inside the pressure chamber. The experiment was conducted at a constant temperature to preserve the dynamics of the PO_4 groups under elevated pressure. Measurements were taken during the pressure increase.

The alternating current (AC) electric conductivity was measured using AC impedance spectroscopy under various isobaric conditions (from 0.1 to 400 MPa). Measurements were carried out with the AC admittance method using a Hewlett-Packard 4284A Precision LCR meter in the frequency range from 100 Hz to 1 MHz and in the temperature range from 330 to 417 K.

3. Results and discussion

3.1. The impact of hydrostatic pressure

The AC conductivity of the $CsH_5(PO_4)_2$ single crystal was measured across a frequency range from 100 Hz to 1 MHz, at temperatures ranging from 200 to 420 K, and at pressures ranging from 0.1 to 360 MPa. The pressure was increased in small steps, and changes in the crystal's conductivity were monitored at regular intervals after each pressure increase. The data were used to identify the optimal thermodynamic conditions for spontaneous transformation from the low-conductivity phase to the high-conductivity phase.

Applying high pressure causes the crystal compression, shortens the hydrogen bond, and thus alters the potential for proton movement within it. It also reduces the distances between molecules (or ions), likely strengthening local interactions. This was clearly demonstrated in the experiment by Meier et al. [29]. Even low pressure significantly influences bond lengths, angles, and ion mobility [30–33], resulting in a more rigid and ordered structure. Specifically, proton diffusion decreases, leading to reduced conductivity. In our experiment, increasing pressure consistently results in a lower conductivity, σ_{ac}, as shown in Fig. 2.

In the theoretical work by Andriyevsky et al. [28], it was shown that the $CsH_5(PO_4)_2$ crystal exhibits anisotropic compressibility due to weakly connected, closely packed planes that promote proton conduction. Because hydrogen bonds are very fragile and sensitive to external conditions, their geometry — such as length and angle — can change

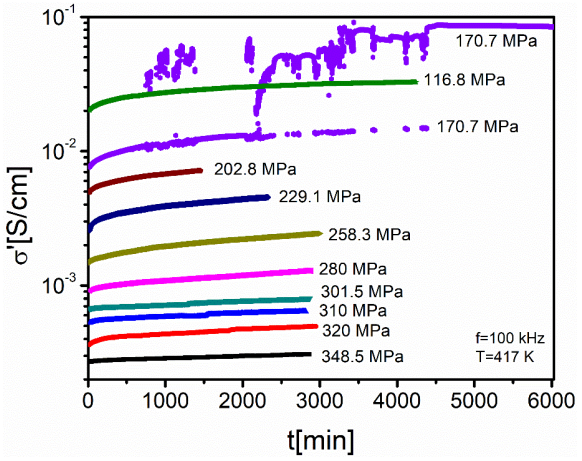

Fig. 2. Time dependence of the AC conductivity measured at $T = 417$ K under varying pressure values and a frequency of 100 Hz.

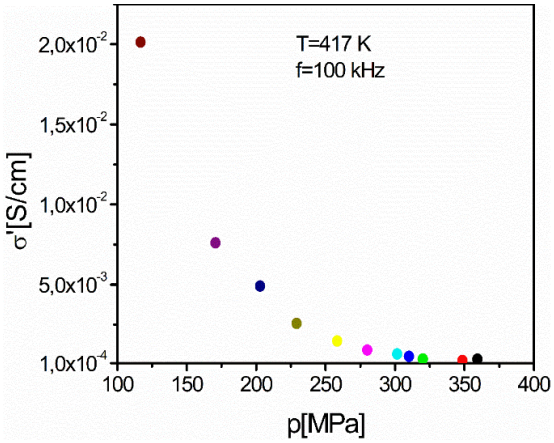

Fig. 3. Initial conductivity of the crystal as a function of pressure.

even at low pressures. Under pressure, hydrogen bonds tend to shorten, decreasing both their length and proton conductivity [30–33]. These effects are illustrated in Fig. 3. The pressure dependence follows the model described in [10, 34–37], which can reproduce the results shown in Fig. 3, although it does not accurately capture the behavior at 170.7 MPa — the focus of this study.

At each pressure, the conductivity initially remains relatively stable for less than 10 h. After this period, under constant thermodynamic conditions ($p = 170.7$ MPa, $T = 417$ K), the protonic conductivity of $CsH_5(PO_4)_2$ crystals shows an unexpected and significant change over time (see Fig. 2).

After releasing the pressure to atmospheric levels, the measurements were repeated for the whole pressure range using the same crystal sample without disassembling the pressure chamber. The conductivity anomaly was again observed under the same conditions ($p = 170.7$ MPa, $T = 417$ K), but was more pronounced. It increases after 300 h, reaching a saturation point ten times its original level. This growth occurs unpredictably and is characterized by significant fluctuations, often accompanied by notable drops following substantial gains. Later observations show a gradual decrease in conductivity over time. The results are shown in Fig. 4.

3.2. Modeling

To justify the proposed conductivity mechanism, we present a numerical model that can partially qualitatively reproduce the observed time dependence of conductivity along the c-axis. We consider a three-dimensional square lattice of size N^3, representing possible positions of H bonds. Since describing the time evolution of diffusing protons in the crystal is a complex process that, even when treated approximately, requires significant computational resources, we only model the evolution of conducting paths, not the protons' movements. Figure 5 presents a schematic illustration of the lattice with a conducting path. The conductivity along a path is determined under the assumption of constant motion of all protons belonging to that path. We also assume that the time steps in our simulation are long enough for protons to diffuse from the initial surface to the final one. This also means that the granularity of time in our considerations is much larger than all the characteristic times of the sub-processes that create the overall diffusion.

In detail, taking into account that H bonds between high-conductivity planes are acceptor-bifurcated, we assume:

(i) H-bonds can form and break near conducting paths between high-conductivity planes.

(ii) H-bonds can form and break spontaneously in the bulk between high-conductivity planes.

These points (i)–(ii) demonstrate the existence of metastable bonds postulated by Merinov [22]. The creation or destruction of metastable bonds can be caused by small disturbances resulting from a protonic current flow (on the microscopic scale) or an applied voltage (in the bulk). A new H bond formed in one step may not immediately become part of any path. When we simulate direct current (DC) conductivity, such a bond may appear artificial, as for DC current only percolation paths are important. However, from the perspective of AC current, even very short incomplete paths contribute to AC conductivity. Therefore, it is physically reasonable to allow the existence of H bonds that are not part of any path. During evolution, these bonds may help form new paths or modify existing ones. We do not model AC conductivity,

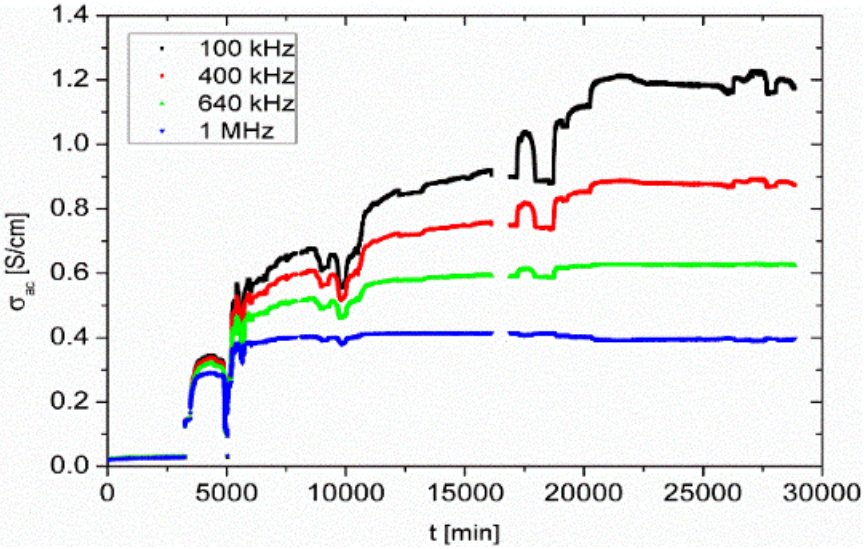

Fig. 4. Time dependence of the AC conductivity measured at $T = 417$ K at constant pressure 170.7 MPa.

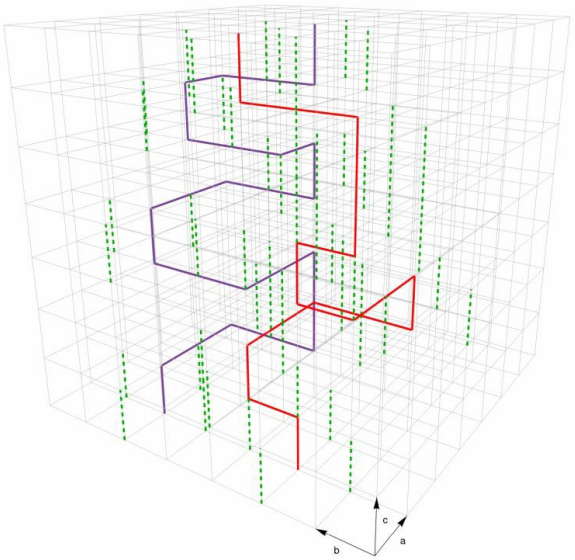

Fig. 5. Two representative conduction paths (red and violet polylines) are shown, along with links indicating sites where new H bonds may be formed during the next simulation step (green dashed lines). Crystallographic axes are displayed at the bottom.

as it requires significantly more computational resources even in simple one-dimensional models [37].

(iii) An H bond connecting two adjacent planes (i.e., a bond along the c axis) can be part of only one conducting path, whereas proton diffusion within high-conductivity planes is always possible between any two points.

This assumption arises from the difference in frequencies characteristic for proton hopping between high-conductivity planes and within them. By hopping, we mean all processes that result in elementary displacement of protons during diffusion.

(iv) The initial density of the hydrogen-bond network is low, near the percolation threshold.

(v) Certain positions in the lattice cannot form H bonds because they are lattice defects.

These points are technical, and we also considered their zero limit (i.e., no initially existing H bonds along the c-axis and no defects). In each step of the evolution, we allow all conducting paths to be generated anew, using all existing H bonds. The zeroth approximation of the DC current is the number of conducting paths, but this approach does not consider that paths may have different lengths or that the proton travel times can vary between paths. Therefore, we express the proton current as

$$j = \frac{1}{N^2\, l_{(001)}^2} \sum\nolimits_{k \in \text{paths}} n_k v_k, \tag{1}$$

where n_k and v_k are the number of protons involved in charge transport and the average velocity of protons along path k, respectively. Note that n_k and v_k can be expressed in terms of lattice parameters and characteristic quantities describing the diffusion process. The number of protons involved in diffusion depends on the number of H bonds in the (001) plane (the high conductivity plane) and the number of H-bonds oriented toward the c-axis (a low conductivity direction). This is written as

$$n_k = N_c\, n_k^c + N_k^{(001)} n_k^{(001)}, \tag{2}$$

where $N_c = N - 1$ and $N_k^{(001)}$ represent the numbers of H bonds toward the c-axis and along the (001) planes, respectively, while n_k^c and $n_k^{(001)}$ denote the numbers of protons involved in transport

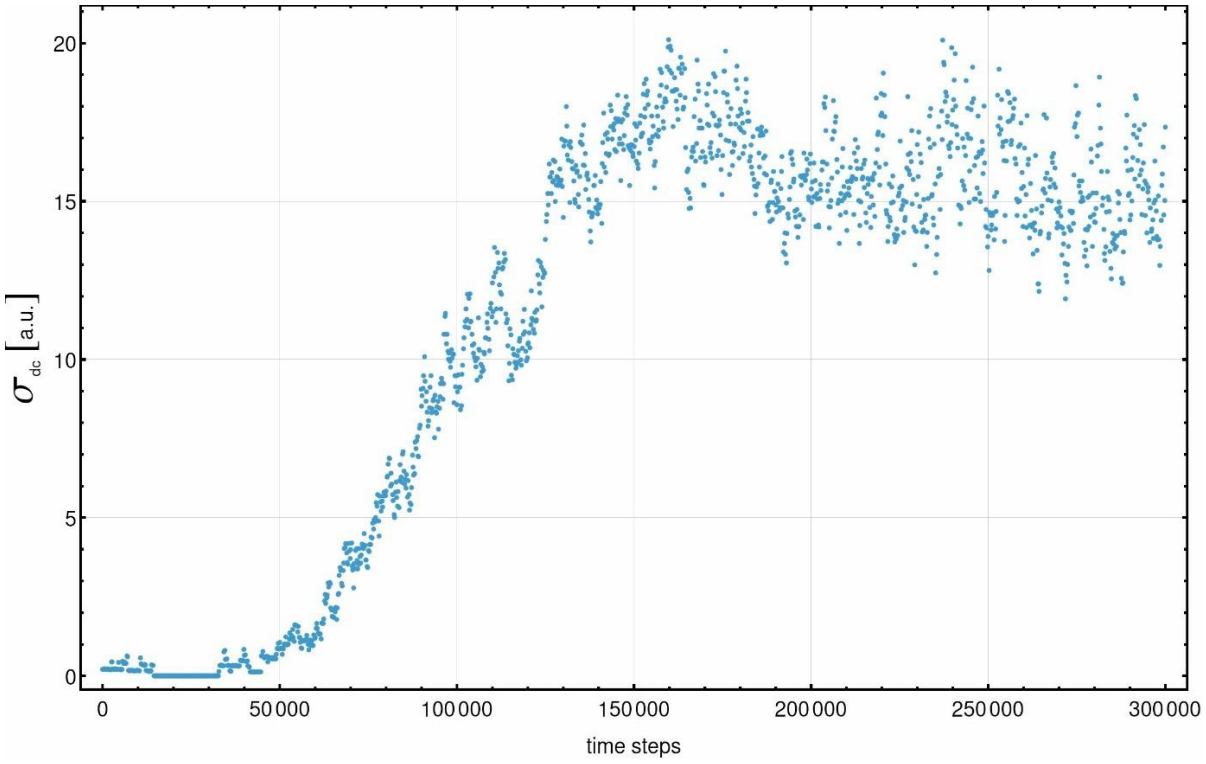

Fig. 6. Conductivity behavior for a lattice of size 50^3 with 300000 time steps. The probability of H-bond creation or destruction near the conducting path is of the order of 10^{-4}, while in the bulk it is 10^{-9}. The characteristic initial plateau and significant growth with high jumps match the experimental observations.

along path k. Since we assume that diffusion occurs along a single path, we set $n_k^c = n_k^{(001)}$, which reflects the dominant ratio of the average number of hydrogen-bonded oxygen atoms to the number of XO_4 tetrahedra in the chains within the hydrogen-bonded networks of solid acids. We approximate the average proton velocity on path k by

$$v_k = \frac{N_c\, l_c + N_k^{(001)}\, l_{(001)}}{N_c\, t_c + N_k^{(001)}\, t_{(001)}}, \tag{3}$$

where l_c and $l_{(001)}$ represent the lattice parameters, and t_c and $t_{(001)}$ are the characteristic hopping times. During simulations, we set $l_c = 2l_{(001)}$ and $t_c = 10t_{(001)}$. Thus, the current j is determined only by the ratios $n_k^c/n_k^{(001)}$, $l_c/l_{(001)}$, and $t_c/t_{(001)}$, while the specific values of these parameters only affect the factor in front of (1).

A typical simulation result is shown in Fig. 6. It shows qualitative similarities to the experimental data, with an initially almost constant behavior and a growth that fluctuates randomly around the average conductivity over time.

Based on the simulations, we can categorize the evolution into three phases. In the first phase, the process is driven by the bulk behavior. This stage involves weak, metastable bonds, slightly disturbed by the altered voltage, finding their energy minima through the formation of H bond. When the number of H bonds surpasses the percolation threshold, conducting paths emerge, and the system enters the second phase, in which it is driven by the formation and breaking of H bonds near these paths. This process is much more efficient, resulting in a rapid and unpredictable increase in conductivity. The third and final phase arises from the optimization of paths and the establishment of dynamical equilibrium.

4. Conclusions

Using impedance spectroscopy, we examined the proton-conducting $CsH_5(PO_4)_2$ crystal to determine whether slight changes in its crystal structure and proton mobility, caused by external pressure, lead to a transition to its highly conductive phase. The AC conductivity was measured across a frequency range from 100 Hz to 1 MHz, at temperatures ranging from 200 to 420 K, and pressures ranging from 0.1 to 360 MPa.

Under specific thermodynamic conditions ($p = 170.7$ MPa, $T = 417$ K), the protonic conductivity of the $CsH_5(PO_4)_2$ crystal for the low-conductivity direction shows an unexpected and significant change over time. The conductivity remains constant for short periods, less than 10 h. After that, for up to 300 h, there is a phase of conductivity increase that saturates at

ten times its initial value. This growth occurs quite randomly, with major drops following large rises. Further observations reveal a gradual decline in conductivity.

The increase in conductivity happens because of the formation of "supplementary" hydrogen bonds between the high-conductivity layers, forming a percolation path perpendicular to these planes.

A model was developed to reproduce the experimentally observed time-dependent conductivity. Initially, it showed little progress, then had a step-like increase, and finally a slight decrease. Path optimization reduces the concentration because protons mainly come from regions with high conductivity.

A numerical model was developed to reproduce the experimentally observed changes in proton conductivity over time under specific thermodynamic conditions ($p = 170.7$ MPa, $T = 417$ K). The simulated conductivity initially increased slowly, then exhibited distinct step-like jumps, and finally showed a slight decrease. This pattern can be explained by the optimization of conduction pathways, which gradually reduces the overall proton concentration as protons are mostly depleted from regions with high conductivity. The long-term conductivity behavior depends on the balance between the number of conductive pathways and their concentration.

Acknowledgments

The authors thank Professor V.G. Ponomareva and Dr. G.V. Lavrova, from the Institute of Solid State Chemistry, Siberian Branch of the Russian Academy of Sciences in Novosibirsk, for providing $CsH_5(PO_4)_2$ crystals for research.

We would like to thank Engineer Z.J. Frączek for his technical assistance.

References

[1] A. Shivhare, A. Kumar, R. Srivastava, *Green Chem.* **23**, 3818 (2021).

[2] H. Zhao, Z.-Y. Yuan, *ChemCatChem* **12**, 3797 (2020).

[3] L. Chen, Y. Zhao, J. Yang, D. Liu, X. Wei, X. Wang, Y. Zheng, *Inorg. Chem.* **59**, 1566 (2020).

[4] A. Goñi-Urtiaga, D. Presvytes, K. Scott, *Hydrog. Energy* **37**, 3358 (2012).

[5] O. Paschos, J. Kunze, U. Stimming, F. Maglia, *J. Phys. Condens. Matter* **23**, 234110 (2011).

[6] S.M. Haile, C.R.I. Chisholm, K. Sasaki, D.A. Boysen, T. Uda, *Faraday Discuss.* **134**, 17 (2007).

[7] Q. Cheng, X. Zhao, G. Yang, L. Mao, F. Liao, F. Chen, P. He, D. Pan, S. Chen, *Energy Storage Mater.* **41**, 842 (2021).

[8] W. Habraken, P. Habibovic, M. Epple, M. Bohner, *Mater. Today* **19**, 69 (2015).

[9] K.D. Kreuer, A. Rabenau, W. Weppner, *Angewandte Chemie Int.* **21**, 208 (1982).

[10] T. Masłowski, A. Drzewiński, P. Ławniczak, M. Zdanowska-Frączek, J. Ulner, *Solid State Ion.* **278**, 114 (2015).

[11] A.I. Baranov, L.A. Shuvalov, N.M. Schagina, *JETP Lett.* **36**, 381 (1982).

[12] Ph. Colomban, A. Novak, in: *Ph. Colomban (Ed.), Proton Conductors: Solids, Membranes and Gels — Materials and Devices*, Cambridge Univ. Press, Cambridge, 38 (1992).

[13] A.I. Baranov, V.P. Kniznichenko, L.A. Shuvalov, *Ferroelectrics* **100**, 135 (1989).

[14] V.G. Ponomareva, G.V. Lavrova, *Solid State Ionics* **145**, 197 (2001).

[15] G.V. Lavrova, V.G. Ponomareva, *Inorg. Mater.* **38**, 1172 (2002).

[16] S.M. Haile, D.A. Boysen, C.R.I. Chisholm, R.B. Merle, *Nature* **410**, 910 (2001).

[17] D.A. Boysen, T. Uda, C.R.I. Chisholm, S.M. Haile, *Science* **303**, 68 (2004).

[18] T. Uda, S.M. Haile, *Electrochem. Solid-State Lett.* **8**, A245 (2005).

[19] G.V. Lavrova, M.V. Russkih, V.G. Ponomareva, N.F. Uvarov, *Russian Journal of Electrochemistry* **41**, 485 (2005).

[20] D.A. Boysen, S.M. Haile, H. Liu, R.A. Secco, *Chem. Mater.* **15**, 727 (2003).

[21] B.V. Merinov, A.I. Baranov, L.A. Shuvalov, *Sov. Phys. Crystallogr.* **35**, 200 (1990).

[22] B.V. Merinov, *Solid State Ionics* **84**, 89 (1996).

[23] A. Efremov et al., *Russ. J. Inorg. Chem.* **26**, 3213 (1981).

[24] Available at Crystallography Open Database.

[25] G.V. Lavrova, E.B. Burgina, A.A. Matvienko, V.G. Ponomareva, *Solid State Ionics* **177**, 1117 (2006).

[26] V.V. Sinitsin, A.I. Baranov, E.G. Ponyatovskii, *Russ. J. Solid State Phys.* **37**, 1121 (1995).

[27] A. Gradišek, B. Dimnik, S. Vrtnik, M. Wencka, M. Zdanowska-Frączek, G.V. Lavrova, J. Dolinšek, *J. Phys.: Condens. Matter* **23**, 085901 (2011).

[28] B. Andriyevsky, M. Zdanowska-Frączek, *Solid State Ionics* **207**, 14 (2012).

[29] T. Meier, F. Trybel, S. Khandarkhaeva et al., *Nature Commun* **13**, 3042 (2022).

[30] G.A. Samara, T. Sakudo, K. Yoshimitsu, *Phys. Rev. Lett.* **35**, 1767 (1975).

[31] A. Katrusiak, *Phys. Rev. B* **48**, 2992 (1993).

[32] A. Katrusiak, *J. Mol. Struct.* **374**, 177 (1996).

[33] P. Ławniczak, M. Zdanowska-Frączek, Z.J. Frączek, K. Pogorzelec-Glaser, C. Pawlaczyk, *Solid State Ionics.* **225**, 268 (2012).

[34] T. Masłowski, A. Drzewiński, J. Ulner, J. Wojtkiewicz, M. Zdanowska-Frączek, K. Nordlund, A. Kuronen, *Phys. Rev. E* **90**, 012135 (2014).

[35] T. Masłowski, M. Zdanowska-Frączek, Ł. Lindner, *Solid State Ion.* **306**, 20 (2017).

[36] Ł. Lindner, M. Zdanowska-Frązek, A. Pawłowski, Z.J. Frączek, T. Masłowski, *J. Appl. Phys.* **122**, 035105 (2017).

[37] T. Masłowski, *Acta Phys. Pol. A* **135**, 1263 (2019).